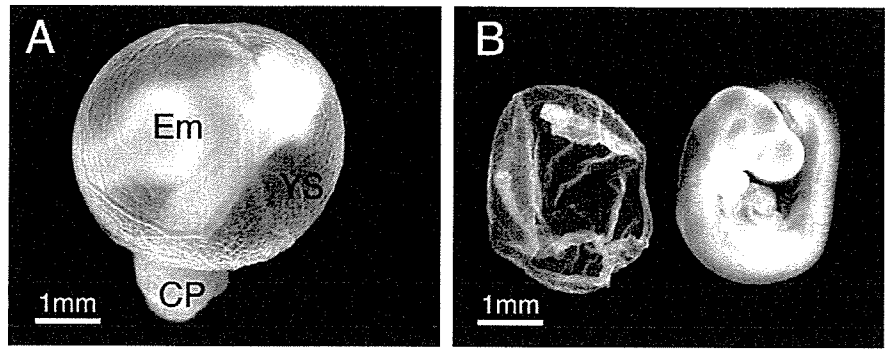

Fig. 1. Appearance of a rat embryo cultured for 24 h from day 10.5 of gestation: (A) At the end of culture. Em, embryo; YS, yolk sac; CP, chorio-allantoic placenta. (B) After the separation of embryonic membranes. Left: yolk sac membrane, Right: embryo.

single gel. The protein spots were identified by mass spectrometry for the construction of a primary 2-DE map of cultured postimplantation rat embryos. The same method could be applied to the 2-DE analysis of yolk sac membranes.

2. Materials and methods

2.1. Embryo culture

Rat embryos were cultured for 24 h by the roller bottle method as previously described (Usami and Ohno, 1996). Embryos were explanted from pregnant Wistar rats (Crlj: WI, Charles River Laboratories Japan, Inc., Kanagawa, Japan) at day 10.5 of gestation (plug day = day 0.5) under ether anesthesia. Explanted embryos were placed in a culture bottle at one embryo per 0.8–1 ml of rat serum and rotated at 35 rpm for 24 h at 37–38 °C. After the culture, the embryos and yolk sac membranes were washed three times with ice-cold buffer (0.01 M Tris–HCl, pH 7.0, 0.15 M NaCl), and placed in 1.5-ml eppendorf tubes individually with a minimum amount of the buffer for storage at −80 °C.

2.2. Preparation of embryo or yolk sac membrane samples

For 2-DE, frozen embryos or yolk sac membranes were lysed in 300 μl of rehydration buffer consisting of 7 M urea, 2 M thiourea, 2% (w/v) CHAPS, 2% (w/v) SB-10, 0.5% (v/v) IPG buffer (Amersham Biosciences, Piscataway, NJ) and 0.12% (v/v) DeStreak Reagent (Amersham Biosciences), by pulsed sonication with a 7-mm ∅ tip immediately after the addition of the buffer. Care was taken to avoid heating and forming during the sonication. Embryo or yolk sac membrane lysates were kept at 20 °C and their protein concentration was determinded with the 2D Quant Kit (Amersham Biosciences).

2.3. Isoelectric focusing (IEF) for the first dimension of 2-DE

IEF was carried out on 13-cm immobilized pH gradient (IPG) strips (Immobiline DryStrip pH 3–10 NL, Amersham Biosciences) with the IPGphor system (Amersham Biosciences). IPG strips were rehydrated with the rehydration buffer containing 50 μg protein of embryo or yolk sac membrane lysate for at least 12 h at 20 °C under a cover with silicon oil. Before the start of IEF, 3-mm-wide IEF electrode strips (Amersham Biosciences) damped were inserted between the IPG strip and both electrodes as electrode pads. Electrophoresis conditions were – Step 1: Step-*n*-hold at 500 V for 1 h, Step 2: Gradient at 1000 V for 1 h, Step 3: Gradient 8000 V for 2.5 h with the current limit of 50 μA per IPG strip. When electrophoresis for the second dimension was not carried out immediately after IEF, the IPG strips were stored at −80 °C.

2.4. Sodium dodecyl sulfate–polyacrylamide gel electrophoresis (SDS–PAGE) for the second dimension of 2-DE

SDS–PAGE was performed according to the method of Laemmli (Laemmli, 1970) except that no stacking gel was used. After IEF, IPG strips were equilibrated with 5 ml of SDS equilibration buffer consisting of 0.05 M Tris–HCl, pH 8.8, 6 M urea, 30% (v/v) glycerol, 2% (w/v) SDS, 0.025% (w/v) bromophenol blue. For the first equilibration, IPG strips were placed in a tube containing equilibration buffer with dithiothreitol (50 mg/5 ml) and rocked for 20 min. For the second equilibration, IPG strips were placed in a tube containing equilibration buffer with iodoacetamide (125 mg/5 ml) and rocked for 20 min. Equilibrated IPG strips were applied onto polyacrylamide gels (12.5% T, 2.6% C, 14 × 6 cm) and sealed with 0.5% agarose in electrode buffer. Electrophoresis was carried at a constant current of

Table 1
Size and protein content of cultured rat embryos

Item	Mean	Standard deviation
Yolk sac diameter (mm)	4.37	0.10
Crown-rump length (mm)	3.99	0.16
Number of somite pairs	26.0	0.67
Embryo protein (μg)	298.2	31.0
Yolk sac protein (μg)	153.0	20.2

Values for 10 embryos are shown.

10 mA per gel for 15 min and thereafter 20 mA per gel until the dye front reached the edge of the gel.

2.5. Stain of 2-DE gel and protein identification

After SDS–PAGE, 2-DE gels were stained with the Plus One Silver Staining Kit Protein (Amersham Biosciences) using the Multi Processor (Amersham Biosciences) according to the manufacturer's instruction. Stained 2-DE gels were scanned and analyzed with the PD Quest 2D analysis software (Bio-Rad, Hercules, CA).

For the identification of protein spots by mass spectrometry, 2-DE gels were stained with the mass-analysis compatible Proteo Silver staining kit (Sigma, St. Louis, MO) and protein spots were excised and cut into 1-mm cubes with a scalpel. Proteins in the gel cubes were digested with trypsin (Shevchenko et al., 1996), cleaned-up with Zip-Tip C18μ (Millipore, Bedford, MA) and analyzed by mass spectrometry using the 4700 Proteomics Analyzer (Applied Biosystems, Foster City, CA). The proteins were identified by the use of mass spectrometry data for the search of primary sequence databases with the MS/MS ion search mode of the Mascot search engine (Matrix Science, Boston, MA).

3. Results

3.1. Embryo culture

Fig. 1A shows a cultured rat embryo at the end of the 24-h culture period. Embryos and yolk sac membranes were separated as samples for 2-DE analysis (Fig. 1B). The amnion and chorio-allantoic placenta were removed and discarded. The size and protein content of the embryos and yolk sac membranes of the cultured rat embryos are shown in Table 1. Protein content in the individual embryo or yolk sac membrane was sufficient for 2-DE anaylsis.

3.2. 2-DE of embryo protein

Proteins of cultured embryos were well separated by 2-DE with the present method (Fig. 2). About 800 protein spots were consistently detected in replicate gels each

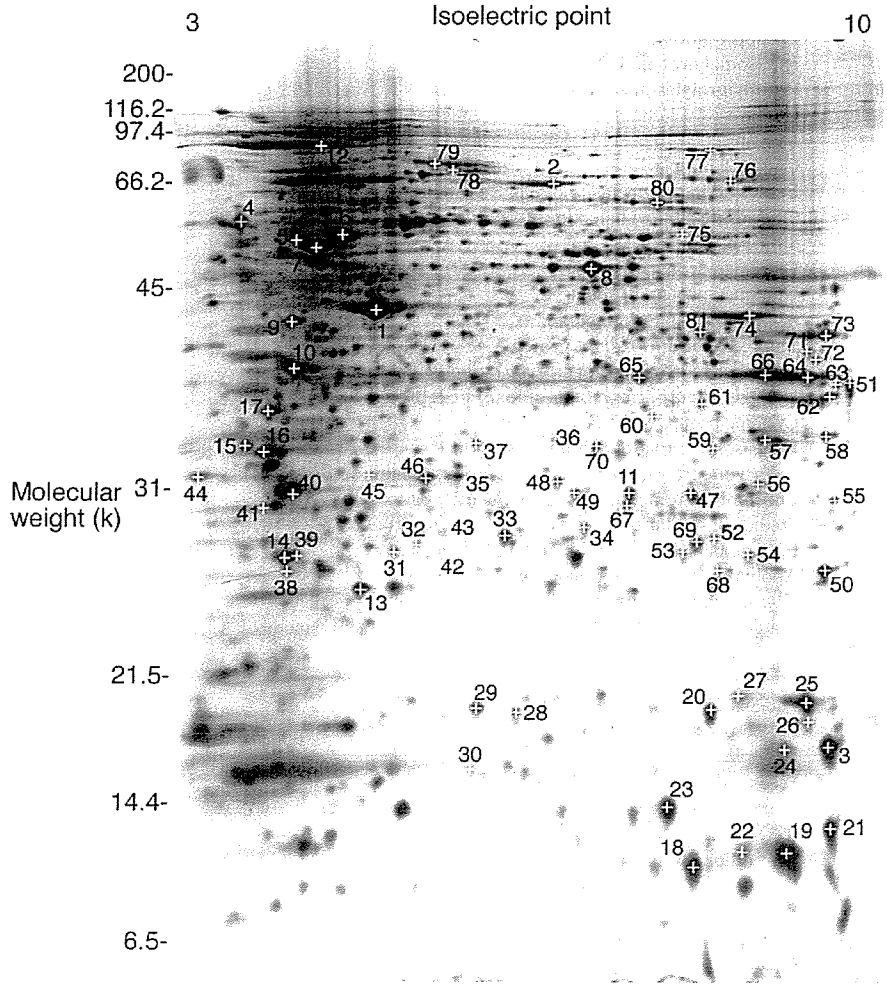

Fig. 2. 2-DE pattern of embryo proteins from a cultured rat embryo equivalent to day 11.5 of gestation. Proteins (50 μg) were separated by IEF with 3–10NL IPG strip (13 cm) and by SDS–PAGE with 12.5% gel (14 × 6 cm), and were stained with silver. Identified protein spots were numbered and listed in Table 2.

Table 2
Protein spots identified in the 2-DE of embryo protein

Spot no.	Accession no.	Protein name	Nominal mass	Calculated pI
1	gi|71620	Actin beta	42,066	5.29
2	gi|19705431	Albumin	70,670	6.09
3	gi|37748460	Peptidylprolyl isomerase A	18,091	8.34
4	gi|11693172	Calreticulin	48,137	4.33
5	gi|202549	Iodothyronine 5′ monodeiodinase	54,375	4.87
6	gi|38014578	Tubulin, beta, 2	50,225	4.79
7	gi|54792127	ATP synthase, H^+ transporting, mitochondrial F1 complex, beta subunit	56,318	5.19
8	gi|38649320	Eno1 protein	51,736	6.70
9	gi|38014840	Laminin receptor 1	32,917	4.80
10	gi|112077	Nucleolar phosphoprotein B23.1	32,711	4.62
11	gi|12844989	Unnamed protein product	28,799	6.67
12	gi|51859516	Heat shock 90 kDa protein 1, beta	83,631	4.97
13	gi|8394432	Peroxiredoxin 2	21,941	5.34
14	gi|6678437	Tumor protein, translationally-controlled 1	19,564	4.76
15	gi|48675371	Complement component 1, q subcomponent binding protein	31,320	4.77
16	gi|34876714	Predicted: similar to Eukaryotic translation elongation factor 1 beta 2	24,831	4.55
17	gi|7242171	Proliferating cell nuclear antigen	29,108	4.66
18	gi|27668426	Predicted: similar to hemoglobin: Subunit = zeta	16,124	6.75
19	gi|3367724	Epsilon 1 globin	16,151	7.90
20	gi|55926145	Expressed in non-metastatic cells 2	17,386	6.92
21	gi|1628436	Profilin	15,149	8.46
22	gi|3367724	Epsilon 1 globin	16,151	7.90
23	gi|40254577	Ribosomal protein S12	14,905	6.81
24	gi|37748460	Peptidylprolyl isomerase A	18,091	8.34
25	gi|509201	Cofilin	18,749	8.22
26	gi|7441446	Destrin	18,661	7.78
27	gi|6671746	Cofilin 2, muscle	18,812	7.66
28	gi|19924089	Expressed in non-metastatic cells 1, protein (NM23A) (nucleoside diphosphate kinase)	17,296	5.96
29	gi|38328242	Stmn1 protein	17,278	5.76
30	gi|12850597	Unnamed protein product	17,138	5.95
31	gi|57006	Unnamed protein product	22,320	5.55
32	gi|202945	Apolipoprotein A-I precursor	30,100	5.52
33	gi|3688521	Thiol-specific antioxidant protein	24,860	5.64
34	gi|8394082	Proteasome (prosome, macropain) subunit, beta type 3	23,235	6.15
35	gi|20071222	NADH dehydrogenase (ubiquinone) Fe-S protein 3	30,358	6.40
36	gi|1381643	Cysteine protease p32-beta	30,097	5.68
37	gi|30410794	Proteasome activator subunit 3 isoform 1	29,602	5.69
38	gi|21312044	Eukaryotic translation initiation factor 3, subunit 12	25,356	4.81
39	gi|6671696	Chromobox homolog 1 (Drosophila HP1 beta)	21,519	4.85
40	gi|27664664	Predicted: similar to 25 kda FK506-binding protein	25,220	9.29
41	gi|6381991	Integrin beta 4 binding protein	27,007	4.63
42	gi|202945	Apolipoprotein A-I precursor	30,100	5.52
43	gi|2897818	Huntingtin interacting protein-2	22,503	5.33
44	gi|6978499	Acidic (leucine-rich) nuclear phosphoprotein 32 family, member A	28,718	3.99
45	gi|47169488	TPA: proteasome subunit alpha type 3-like	28,621	5.19
46	gi|62664759	Predicted: prohibitin	27,757	5.44
47	gi|297111	Phosphoglyceromutase	28,908	8.85
48	gi|16758298	Proteasome (prosome, macropain) subunit, beta type 7	30,250	8.13
49	gi|16758848	Endoplasmic retuclum protein 29	28,614	6.23
50	gi|56789700	Peroxiredoxin 1	22,323	8.27
51	gi|38648863	Malate dehydrogenase, mitochondrial	36,117	8.93
52	gi|16758182	RAN, member RAS oncogene family	24,579	7.01
53	gi|5420030	Glutathione transferase	25,550	6.77
54	gi|25453420	Glutathione S-transferase, pi	23,652	6.89
55	gi|56550075	Proteasome (prosome, macropain) subunit, alpha type 7	28,010	8.60
56	gi|8394069	Proteasome (prosome, macropain) subunit, alpha type 4	29,764	7.59
57	gi|18543331	Guanine nucleotide binding protein, beta polypeptide 2-like 1	35,529	7.60
58	gi|38051979	Vdac1 protein	32,060	8.35
59	gi|1906812	Inducible carbonyl reductase	30,920	7.64
60	gi|62661724	Predicted: similar to esterase D/formylglutathione hydrolase	37,322	6.45

Table 2 (*continued*)

Spot no.	Accession no.	Protein name	Nominal mass	Calculated pI
61	gi|57527447	Ribose-phosphate pyrophosphokinase I -like	35,297	6.51
62	gi|54261548	Lactate dehydrogenase A	36,712	8.45
63	gi|7949053	Heterogeneous nuclear ribonucleoprotein A2/B1 isoform 1	36,028	8.67
64	gi|62653546	Predicted: similar to glyceraldehyde-3-phosphate dehydrogenase	36,045	8.44
65	gi|6978491	Aldehyde reductase 1	36,230	6.26
66	gi|62653546	Predicted: similar to glyceraldehyde-3-phosphate dehydrogenase	36,045	8.44
67	gi|76647405	Predicted: similar to proteasome subunit alpha type 6 (proteasome iota chain) (macropain iota chain)	27,838	6.34
68	gi|8394079	Proteasome (prosome, macropain) subunit, beta type 2	23,069	6.96
69	gi|8394063	Proteasome (prosome, macropain) subunit, alpha type 2	26,024	6.92
70	gi|62655706	Predicted: similar to RIKEN cdna 1110025F24	26,482	5.90
71	gi|61889115	Phosphoserine aminotransferase 1	40,943	7.57
72	gi|66911068	Pcbp2_predicted protein	35,666	8.17
73	gi|202837	Aldolase A	39,691	8.31
74	gi|38649310	Phosphoglycerate kinase 1	44,909	8.02
75	gi|584875	Adenylyl cyclase-associated protein 1 (CAP 1)	51,857	7.16
76	gi|74144333	Unnamed protein product	67,573	7.18
77	gi|19424312	KH-type splicing regulatory protein	74,466	6.38
78	gi|228784	Alpha fetoprotein	70,167	5.71
79	gi|228784	Alpha fetoprotein	70,167	5.71
80	gi|2511703	p60 protein	63,158	6.40
81	gi|2644966	hnRNP-E1 protein	37,987	6.66

Proteins names with their NCBI accession numbers were shown for the protein spots in Fig. 1.

from one embryo. Selected protein spots were analyzed by mass spectrometry and 81 protein spots were identified as shown in Table 2. These protein spots also served as landmarks for the matching of protein spots among the gels.

3.3. 2-DE of yolk sac membrane protein

Proteins of yolk sac membranes were separated as well as those of embryos by 2-DE with the present method (Fig. 3). The 2-DE pattern of yolk sac membranes was fairly different from that of embryos. Most protein spots were common but were quantitatively different between the yolk sac membranes and the embryos. In addition, there were embryo specific and yolk sac membrane specific protein spots.

4. Discussion

The present method is simple and can be carried out concomitantly with in vitro developmental toxicity studies using rat embryo culture. The whole 2-DE procedures are completed within four days. IPG strips with narrower pH ranges would be useful for precise and convenient analysis of specific protein spots. For screening purposes or focused proteomics, the same procedures could be applied to the mini-gel format with shorter IPG strip and mini SDS–PAGE gel.

The primary 2-DE map constructed in the present study is useful for interlaboratory comparison of 2-DE patterns. Abundant and characteristic protein spots can be used as landmarks for matching of the 2-DE pattern. We are planning to identify more protein spots for a more precise and accurate 2-DE map of cultured rat embryos in future, giving priority to protein spots of interest that are differentially expressed due to the effects of developmental toxicants. Identification of very faint protein spots may require a separate 2-DE experiment with an increased amount of applied protein samples.

It is expected that 2-DE analysis by the present method enables informative experiments for developmental toxicity studies. Because protein from less than one embryo is sufficient for 2-DE analysis in the present method, toxic effects observed in individual embryos may be related to the changes in protein expression pattern. Alternatively, analysis of specific parts isolated from single embryos may improve the efficiency of differential analysis. It is also noted that the present method is valid for 2-DE analysis of yolk sac membranes as well as embryos. Simultaneous analysis of yolk sac membranes with embryos would be useful to investigate the action sites of developmental toxicants.

The critical point of the present method is the use of the DeStreak Reagent as an antioxidant and the electrode pads. Both of which greatly improved the 2-DE pattern by decreasing horizontal streaks in the present method. We initially used dithiothreitol or tributylphosphine as a reducing agent to avoid the oxidation of proteins but could not decrease the streaks sufficiently. High concentration of redox agents such as glutathione in the embryo or yolk sac membrane samples (Harris et al., 1995) might affect redox status of proteins when dithiothreitol or tributylphosphine was used.

As far as we tested, addition of protease inhibitors to the lysis/rehydration buffer had no effects on the 2-DE pattern. It is considered that the constituents of the lysis/rehydration buffer were effective for inactivation of proteases in the

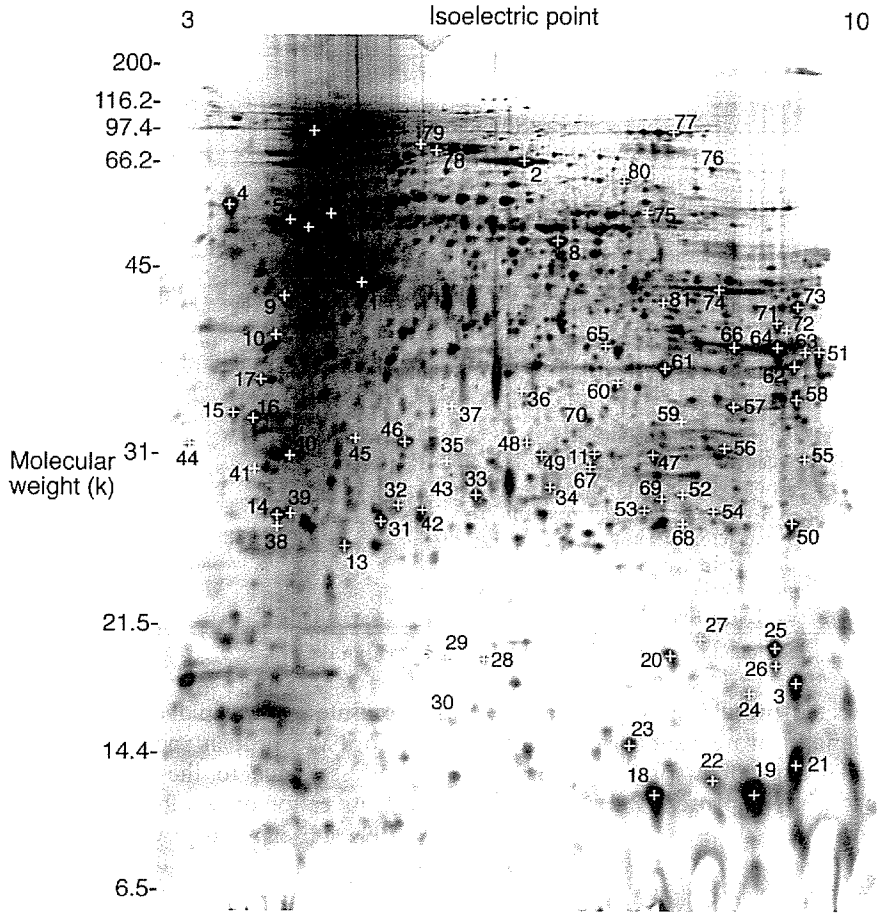

Fig. 3. 2-DE pattern of yolk sac membrane proteins from a cultured rat embryo equivalent to day 11.5 of gestation. Proteins (50 μg) were separated by IEF with 3–10NL IPG strip (13 cm) and by SDS–PAGE with 12.5% gel (14 × 6 cm), and were stained with silver. Proteins identified for the embryo are indicated by the same number as in Fig. 2.

embryo or yolk sac membrane samples. No requirement for protease inhibitors in the present method saves the const and labor in the 2-DE analysis.

In conclusion, it is considered that the present method is suitable for 2-DE analysis of embryos and yolk sac membranes in developmental toxicity studies using postimlantation rat embryo culture.

Acknowledgements

This work was partially supported by the Ministry of Education, Science, Sports and Culture, Grant-in-Aid for Exploratory Research, 15658090, 2003–2005.

References

Baumgartner, B.G., Murach, K.-F., Schlegel, E., Praxmayer, C., Illmensee, K., 1994. Comparison of protein analysis between embryonic and extraembryonic tissues during the 11th day of gestation of the mouse. Electrophoresis 15, 992–1000.

Fountoulakis, M., Berndt, P., Boelsterli, U.A., Crameri, F., Winter, M., Albertini, S., Suter, L., 2000. Two-dimensional database of mouse liver proteins: Changes in hepatic protein levels following treatment with acetaminophen or its nontoxic regioisomer 3-acetamidophenol. Electrophoresis 21, 2148–2161.

Greene, N.D.E., Leung, K.-Y., Wait, R., Begum, S., Dunn, M.J., Copp, A.J., 2002. Differential protein expression at the stage of neural tube closure in the mouse embryo. J. Biol. Chem. 277, 41645–41651.

Harris, C., Hiranruengchok, R., Lee, E., Berberian, R.M., Eurich, G.E., 1995. Glutathione status in chemical embryotoxicity: Synthesis, turnover and adduct formation. Toxicol. in Vitro 9, 623–631.

Laemmli, U.K., 1970. Cleavage of structural proteins during the assembly of the head of bacteriophage T4. Nature 227, 680–685.

Piubelli, C., Cecconi, D., Astner, H., Caldara, F., Tessari, M., Carboni, L., Hamdan, M., Righetti, P.G., Domenici, E., 2005. Proteomic changes in rat serum, polymorphonuclear and mononuclear leukocytes after chronic nicotine administration. Proteomics 5, 1382–1394.

Praxmayer, C., Murach, K.-F., Baumgartner, B., Aberger, F., Schlegel, E., Illmensee, K., 1992. Protein synthesis in murine organs during postimplantation development detected by two-dimensional gel electrophoresis. Electrophoresis 13, 720–722.

Schmid, B., Bechter, R., Kucera, P., 1997. Use of whole emryo cultures in in vitro teratogenicity testing. In: Castell, J.V., Gómez-Lechón, M.J. (Eds.), In Vitro Methods in Pharmacetical Research. Academic Press, San Diego, pp. 353–373.

Shevchenko, A., Wilm, M., Vorm, O., Mann, M., 1996. Mass spectrometric sequencing of proteins from silver-stained polyacrylamide gels. Anal. Chem. 68, 850–858.

Usami, M., Ohno, Y., 1996. Teratogenic effects of selenium compounds on cultured postimplantation rat embryos. Teratog. Carcinog. Mutagen. 16, 27–36.

Xu, H., Hu, L.S., Chang, M., Jing, L., Zhang, X.Y., Li, G.S., 2005. Proteomic analysis of kidney in fluoride-treated rat. Toxicol. Lett. 160, 69–75.

Am J Physiol Heart Circ Physiol 290: H1660–H1670, 2006.
First published November 4, 2005; doi:10.1152/ajpheart.00100.2004.

Multiple transcripts of Ca^{2+} channel α_1-subunits and a novel spliced variant of the α_{1C}-subunit in rat ductus arteriosus

Utako Yokoyama,[1,2] Susumu Minamisawa,[2,4] Satomi Adachi-Akahane,[5] Toru Akaike,[1] Isao Naguro,[6] Kengo Funakoshi,[3] Mari Iwamoto,[1] Masamichi Nakagome,[2] Nobuyuki Uemura,[2] Hideaki Hori,[2] Shumpei Yokota,[1] and Yoshihiro Ishikawa[2,7]

Departments of [1]Pediatrics, [2]Physiology, and [3]Neuroanatomy, Yokohama City University, Yokohama; [4]Consolidated Research Institute for Advanced Science and Medical Care, Waseda University; [5]Department of Pharmacology, School of Medicine, Faculty of Medicine, Toho University, Tokyo; [6]Laboratory of Cell Signaling, Graduate School of Pharmaceutical Sciences, The University of Tokyo, Tokyo, Japan; and [7]Cardiovascular Research Institute, Departments of Cell Biology and Molecular Medicine and Medicine (Cardiology), New Jersey Medical School, Newark, New Jersey

Submitted 3 February 2004; accepted in final form 27 October 2005

Yokoyama, Utako, Susumu Minamisawa, Satomi Adachi-Akahane, Toru Akaike, Isao Naguro, Kengo Funakoshi, Mari Iwamoto, Masamichi Nakagome, Nobuyuki Uemura, Hideaki Hori, Shumpei Yokota, and Yoshihiro Ishikawa. Multiple transcripts of Ca^{2+} channel α_1-subunits and a novel spliced variant of the α_{1C}-subunit in rat ductus arteriosus. *Am J Physiol Heart Circ Physiol* 290: H1660–H1670, 2006. First published November 4, 2005; doi:10.1152/ajpheart.00100.2004.—Voltage-dependent Ca^{2+} channels (VDCCs), which consist of multiple subtypes, regulate vascular tone in developing arterial smooth muscle, including the ductus arteriosus (DA). First, we examined the expression of VDCC subunits in the Wistar rat DA during development. Among α_1-subunits, α_{1C} and α_{1G} were the most predominant isoforms. Maternal administration of vitamin A significantly increased α_{1C}- and α_{1G}-transcripts. Second, we examined the effect of VDCC subunits on proliferation of DA smooth muscle cells. We found that 1 μM nitrendipine (an L-type Ca^{2+} channel blocker) and kurtoxin (a T-type Ca^{2+} channel blocker) significantly decreased [^{3}H]thymidine incorporation and that 3 μM efonidipine (an L- and T-type Ca^{2+} channel blocker) further decreased [^{3}H]thymidine incorporation, suggesting that L- and T-type Ca^{2+} channels are involved in smooth muscle cell proliferation in the DA. Third, we found that a novel alternatively spliced variant of the α_{1C}-isoform was highly expressed in the neointimal cushion of the DA, where proliferating and migrating smooth muscle cells are abundant. The basic channel properties of the spliced variant did not differ from those of the conventional α_{1C}-subunit. We conclude that multiple VDCC subunits were identified in the DA, and, in particular, α_{1C}- and α_{1G}-subunits were predominant in the DA. A novel spliced variant of the α_{1C}-subunit gene may play a distinct role in neointimal cushion formation in the DA.

alternative spliced; development; gene expression; fetal circulation

THE DUCTUS ARTERIOSUS (DA) is a fetal arterial connection between the pulmonary artery and the descending aorta. After birth, the DA closes immediately, in accordance with its smooth muscle contraction. An increase in oxygen tension and a dramatic decline in circulating prostaglandins are the most important triggers of DA contraction (5). Generally, vascular smooth muscle contraction is induced by Ca^{2+}/calmodulin-dependent phosphorylation of the regulatory myosin light chain, which is mediated by an increase in intracellular Ca^{2+}. Ca^{2+} influx through voltage-dependent Ca^{2+} channels (VDCCs) and Ca^{2+} release from intracellular stores are major sources of this increase (8, 26). Thus VDCCs must play an important role in vascular myogenic reactivity and tone of the DA.

VDCCs are classified, according to their distinct electrophysiological and pharmacological properties, into low (T-type) and high (L-, N-, P-, Q-, and R-type) VDCCs (20, 39). VDCCs consist of different combinations of α_1-subunits and auxiliary subunits. The α_1-subunit forms the ion-conducting pore, the voltage sensor, and the interaction sites for Ca^{2+} channel blockers and activators (15). Therefore, α_1-subunits principally determine the channel character of VDCCs. Ten α_1-subunit isoforms have been identified. Four $\alpha_{2\delta}$-subunit complexes and four β-subunits, which modulate the trafficking and the biophysical channel properties of α_1-subunits (1), have been identified (3). Although some studies have investigated the role of VDCCs in the DA (28, 37), characterization of VDCCs, including the composition of each subunit, the developmental change in their expression, and their physiological roles, remains poorly understood.

In addition to their role in determining contractile state, a growing body of evidence has demonstrated that VDCCs play an important role in regulating differentiation and remodeling of vascular smooth muscle cells (SMCs) (14, 17, 41). The DA dramatically changes its morphology during development. Intimal cushion formation during development is a characteristic feature of vascular remodeling of the DA (10, 30). Intimal cushion formation involves many cellular processes, including an increase in SMC migration and proliferation, production of hyaluronic acid under the endothelial layer, and impairment of elastin fiber assembly. The role of VDCCs in vascular remodeling of the DA has not been investigated.

In the present study, we identified multiple VDCC subunits in the DA by semiquantitative and quantitative RT-PCR and immunodetection. In particular, α_{1C}- and α_{1G}-subunits were predominant in the DA. Furthermore, we will demonstrate the identification of a novel spliced variant of the α_{1C}-subunit gene that may play a role in neointimal cushion formation of the DA.

Address for reprint requests and other correspondence: S. Minamisawa, Dept. of Physiology, Yokohama City Univ., 3-9 Fukuura, Kanazawa-ku, Yokohama 236-0004, Japan (e-mail: sminamis@med.yokohama-cu.ac.jp).

The costs of publication of this article were defrayed in part by the payment of page charges. The article must therefore be hereby marked "*advertisement*" in accordance with 18 U.S.C. Section 1734 solely to indicate this fact.

Table 1. *Oligonucleotides used for RT-PCR*

Gene	Accession No.	Forward (5′-3′)	Position	Reverse (5′-3′)	Position	Size, bp	Annealing Temperature, °C
$Ca_V1.1$ (α_{1S})	U31816	cgcgaggtcatggacgtggag	572–592	gatcaccagccagtagaagac	695–715	144	60
$Ca_V1.2$ (α_{1C})-1	AF394939	ggagagttttccaaagagagg	1342–1362	gatcaccagccagtagaagac	1699–1719	378	60
$Ca_V1.2$ (α_{1C})-2	AF394939	tggaaactcagctctaagag	5551–5570	tcctggtaggagagtatatc	5695–5714	164	54
$Ca_V1.3$ (α_{1D})	NM_017298	attctgaacatggtcttcacg	4246–4265	gattctattgctctcttcaga	4405–4425	180	55
$Ca_V1.4$ (α_{1F})	NM_053701	gcagatggcccttcaatctc	001–020	ccatgtcggatcccaggaag	833–852	852	57
$Ca_V3.1$ (α_{1G})	NM_031601	aatggcaagtcggcttca	3648–3665	caggagacgaaaccttga	3837–3854	207	50
$Ca_V3.2$ (α_{1H})	AF290213	gacgaggataagacgtct	3111–3128	ggagacgcgtagcctgtt	3906–3923	813	57
$Ca_V3.3$ (α_{1I})	NM_020084	gatgaggaccagagctca	2768–2785	tctggctgcagtgagaggc	2943–2961	194	60
$\alpha_{2\delta1}$	NM_012919	tggtgtgatgggcgttgatgtgtc	1741–1764	gtcattgc-agtattcccttggtgc	2234–2258	518	56
$\alpha_{2\delta2}$	NM_175592	aggttcttcagtgaggtggat	2749–2769	ttataggacgcgttcaccgag	3081–3101	353	62
$\alpha_{2\delta3}$	NM_175595	ggcacagatgtcccagtaaaaga	1483–1505	tgtgtagtagtagtcattggtcat	1780–1803	321	58
β_{1-1}	NM_017346	tgacaactccagttccag	624–641	tcaagaagtcaaacaacg	835–852	229	62
β_{1-2}	NM_017346	tcaatgtccaaatagcag	1163–1180	tgtcagcatcaaaggtgtc	1555–1573	411	56
β_2	NM_053851	acagagagcaaagcaagggaat	771–792	tctccttgagaaccctgtgaatt	1693–1715	945	56
β_3	NM_012828	gtggtgttggatgctgac	892–909	attgtggtcatgctccga	1483–1500	609	58
β_4	XM_215742	cgattcggcaagagagagaacagcaag	396–422	gtttgggcagcctcaaagcctatgtcg	1730–1756	1361	58
GAPDH	AF106860	cccatcaccatcttccaggagcg	1060–1082	gcagggatgatgttctgggctgcc	1446–1469	410	55

MATERIALS AND METHODS

Animals. All animals were cared for in compliance with the guiding principles of the American Physiological Society. The experiments were approved by the Ethical Committee of Animal Experiments of Yokohama City University School of Medicine.

Maternal vitamin A administration. Maturation of the fetal DA was accelerated by maternal administration of vitamin A, as described previously (25, 42). Briefly, vitamin A [retinyl palmitate, 33 mg, which is equivalent to 18 mg of retinol (Eisai, Tokyo, Japan)] was diluted in polyoxyethylene castor oil and injected intramuscularly into pregnant Wistar rats daily from *day 17* of gestation in a dose of 1 mg (3,000 IU)/kg body wt.

Tissue collection and preparation. For developmental studies, we used pooled tissues obtained from Wistar rat embryos on embryonic *days 19* (e19, $n = 60$) and *21* (e21, $n = 90$) and from neonates on the day of birth (*day 0*, $n = 60$). After excision, tissues were immediately frozen in liquid nitrogen and stored at −80°C.

Semiquantitative and quantitative RT-PCR. Total RNA was isolated from the tissues using TRIzol, as recommended by the manufacturer (Invitrogen, La Jolla, CA). Genomic DNA was digested by DNase I before RT reaction. After annealing to random hexamer, 2 μM total RNA was reverse transcribed to cDNA by SuperScript II RT (Invitrogen). For semiquantitative RT-PCR analyses of VDCC subunits, the primers for PCR amplification were designed on the basis of the rat nucleotide sequences of VDCCs (Table 1) to amplify cDNA between two exons, except α_{1S}-subunit primers. The PCR cycle consisted of denaturation at 94°C for 30 s, annealing at each temperature for 30 s, and elongation at 72°C for 30 s; 35–40 forty cycles were performed. Amplification products were analyzed by 2% agarose gel electrophoresis and ethidium bromide staining. A fragment of GAPDH was amplified as internal control. For quantitative RT-PCR analysis, sequences for PCR primers are listed in Table 2. The spliced variant of the α_{1C}-subunit and nonspliced isoform were detected simultaneously by $Ca_V1.2$ (α_{1C})-4 primer. Amplification and detection were performed as described previously (40). Each template was tested at least three times to confirm the reproducibility of the assays. The abundance of each gene was determined relative to GAPDH using TaqMan rodent GAPDH control reagents kits (Applied Biosystems, Foster City, CA). For each RT-PCR experiment, we included RT negative control and confirmed no amplification in each reaction.

Restriction enzyme analysis. The relative abundance of high-voltage-activated (HVA) channels of the α_1-subunits was determined in the DA as described previously (29). Briefly, all HVA channels of the α_1-subunits were amplified by RT-PCR using the following set of primers: at(c/t) (a/g)tc acc ttc cag gag ca (forward) and gcg tag atg aag aa(a/g/c) agc at (reverse). Five restriction enzymes selectively cut the α_{1A}-, α_{1B}-, α_{1C}-, α_{1D}-, and α_{1E}-isoforms of the PCR products. The intensity of the digested fragments in correspondence to each isoform was measured by a FujiFilm image analysis system (Image Gauge version 3.41).

Generation of polyclonal antibody against spliced variant of α_{1C}-subunit. We generated a polyclonal antibody against spliced variant of rat α_{1C}-subunit using a keyhole limpet hemocyanin-conjugated synthetic peptide for immunization. Antigens for spliced variant of anti-rat α_{1C}-subunit antibody were derived from the I-II cytoplasmic loop region spanning amino acids 59–71 of the spliced variant of rat

Table 2. *Oligonucleotides used for quantitative RT-PCR*

Gene	Accession No.	Forward (5′-3′)	Position	Reverse (5′-3′)	Position	Probe (5′-3′)	Position	Size, bp
$Ca_V1.2$ (α_{1C})-3	AF394939	tgattgttgtgg-gtagcattgtt	3992–4014	tcatagagggaga-gcattgggtat	4049–4072	tagcaatcaccgaggtacacc-cagctg (FAM)	4019–4072	81
$Ca_V1.2$ (α_{1C})-4	AY323810	aatgaggacgag-ggcatgg	136–154	gcccacaagtgag-actgagtctg	258–280	agggaaatttgcttggtttag-tcactccaca (FAM)	210–241	145
	AF394939					tgaagacaaaccccgaaacat-gagca (VIC)	1497–1522	70
$Ca_V1.3$ (α_{1D})	NM_017298	gaagaggacgag-cctgaggtt	3028–3048	ttttctccttcat-gttcaactctga	3076–3100	(SYBR)		73
$Ca_V3.1$ (α_{1G})	NM_031601	cctgatttctttt-tcgcccag	3054–3073	tggcaaaaggc-tctttcgtag	3138–3158	(SYBR)		105

α_{1C}-subunit (RGAPAGLHDQKKG+C). A male Japanese White rabbit was immunized four times every 2 wk. Serum was collected, and polyclonal antibody was affinity purified.

Immunoblotting. The membrane fraction was prepared and immunoblotting was performed as described previously (23). Briefly, tissues from rat (DA, aorta, atria, left ventricle, and lung) were homogenized in an ice-cold buffer [in mM: 50 Tris (pH 8.0), 1 EDTA, 1 EGTA, 1 dithiothreitol, and 200 sucrose] and protease inhibitors (Complete Mini, Roche, Tokyo, Japan). The polyclonal antibody specific for α_{1C}-, α_{1D}-, and α_{1G}-subunits (Chemicon, Temecula, CA) or spliced variant of α_{1C}-subunit at 5 μg/ml was used to examine 20-μg membrane fractions from rat tissues.

Immunohistochemistry. For immunoperoxidase demonstration of VDCCs in the DA, paraffin-embedded blocks containing DA tissues were cut into 4-μm-thick sections and placed on 3-aminopropyltriethoxysilane-coated glass slides. To determine the boundary line of intimal cushion formation, tissue sections were stained with Elastica van Gieson as recommended by the manufacturer (Muto Pure Chemicals). The specimens were deparaffinized, rehydrated, and incubated for 5 min in peroxidase-blocking reagent (DAKO Laboratories) to inactivate endogenous peroxidases. Slides were incubated with each primary antibody of splicing variant of α_{1C}-, α_{1D}-, α_{1G}-, and α_{1C}-subunits (1:200 dilution) at room temperature for 30 min. After they were washed with 0.1 M PBS for 5 min, the slides were incubated for 30 min in biotinylated rabbit anti-goat IgG (Vector, Burlingame, CA). Then the slides were washed with 0.1 M PBS for 5 min, incubated for 30 min in avidin-biotin-horseradish peroxidase complex (Vector), and washed again with 0.1 M PBS for 5 min. The peroxidase reactivity was demonstrated with 3,3'-diaminobenzidine (Sigma, St. Louis, MO) and 0.3% H_2O_2 for 5 min. The specificity of staining was examined by omission of the primary antibodies. The slides were counterstained with Mayer's hematoxylin.

Primary culture of rat DA SMCs. Vascular SMCs in primary culture were obtained from the DA of Wistar rat embryos at e21. The tissues were minced and transferred to a 1.5-ml centrifuge tube that contained 800 μl of collagenase-dispase enzyme mixture [1.5 mg/ml collagenase-dispase (Roche), 0.5 mg/ml elastase type II-A (Sigma Immunochemicals, St. Louis, MO), 1 mg/ml trypsin inhibitor type I-S (Sigma), and 2 mg/ml bovine serum albumin fraction V (Sigma) in Hanks' balanced salt solution (Sigma)]. The digestion was carried out at 37°C for 15–20 min. Then cell suspensions were centrifuged, and the medium was changed to the collagenase II enzyme mixture [1 mg/ml collagenase II (Worthington), 0.3 mg/ml trypsin inhibitor type I-S, and 2 mg/ml bovine serum albumin fraction V in Hanks' balanced salt solution]. After 12 min of incubation at 37°C, cell suspensions were transferred to growth medium in 35-mm poly-L-lysine (Sigma)-

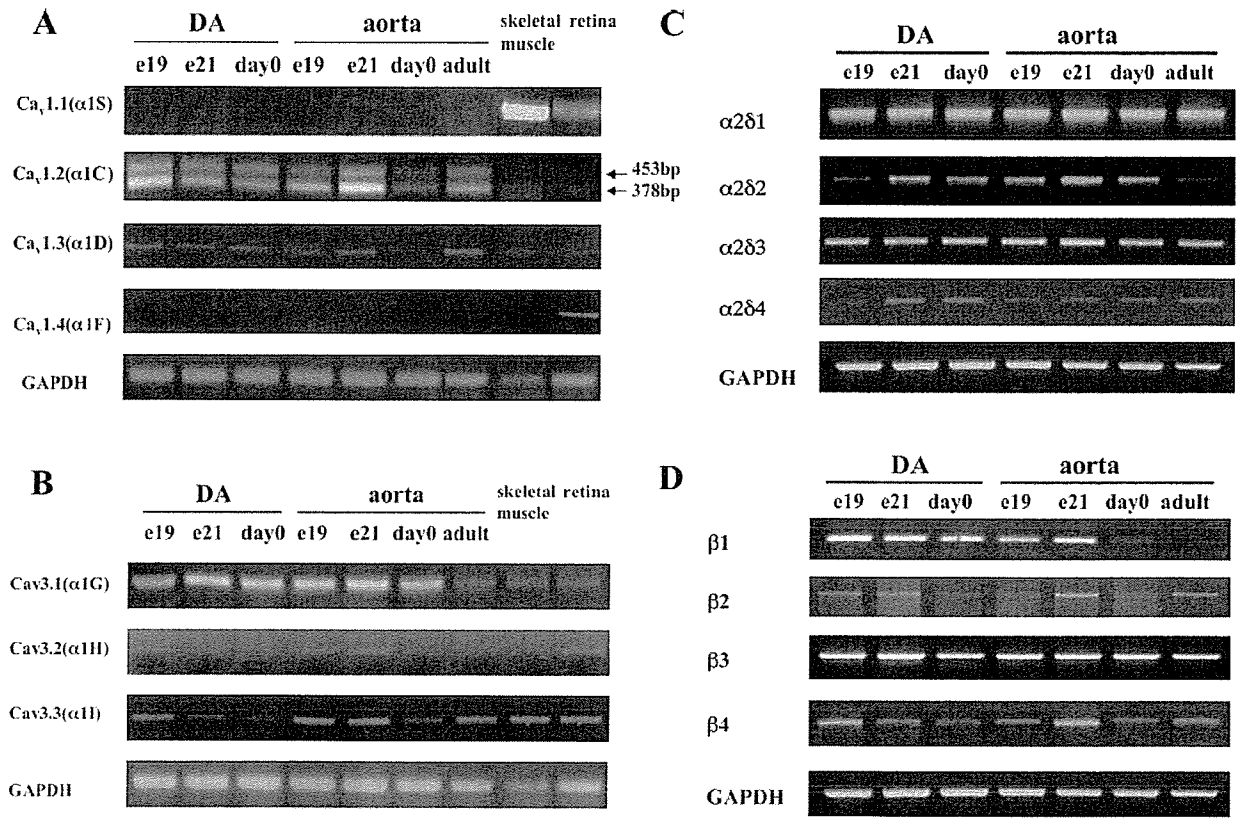

Fig. 1. Semiquantitative RT-PCR analyses of Ca^{2+} channel subunits. *A*: RT-PCR for L-type Ca^{2+} channel α_1-subunit isoforms in rat ductus arteriosus (DA), aorta, skeletal muscle, and retina. RNA samples from tissues were processed for 35 cycles of PCR using primers directed to the cDNA sequence of VDCC α_{1S}-, α_{1C}-, α_{1D}-, and α_{1F}-isoforms. PCR of the primer alone, without template, resulted in no product (data not shown). Transcripts for α_{1C}- and α_{1D}-subunits were detected in DA and aorta, but no transcripts for α_{1S}- and α_{1F}-subunits were detected in DA and aorta. Transcripts for α_{1C}-subunit were detected as clear bands of expected (378 bp) and longer (453 bp) lengths. Sequence analysis detected insertion of an unreported 75-bp cDNA in the 453-bp band into the 378-bp band. Expression of α_{1C}-subunit mRNA was not altered during development. Expression of α_{1D}-subunit mRNA was decreased in DA from embryonic *day 21* (e21) but decreased from *day 0* (birth) in aorta. *B*: RT-PCR for T-type Ca^{2+} channel α_{1G}-, α_{1H}-, and α_{1I}-subunits in rat DA, aorta, skeletal muscle, and retina. Transcripts for these subunits were present in DA and aorta. Expression level of α_{1G}-subunit mRNA was high from embryonic *day 19* (e19) to *day 0* in DA and aorta and decreased in adult aorta. Levels of α_{1H}- and α_{1I}-subunit mRNA expression were low in DA and aorta. *C*: RT-PCR for $\alpha_{2\delta}$-subunits in rat DA and aorta during development. Transcripts for all 4 $\alpha_{2\delta}$-subunit isoforms were present in both tissues. *D*: RT-PCR for β-subunits in rat DA and aorta during development. Transcripts for 4 β-isoforms were present in both tissues. β_3-Subunit mRNA was abundant in DA and aorta throughout development.

coated dishes in a moist tissue culture incubator at 37°C in 5% CO_2-95% ambient mixed air. The growth medium contained DMEM with 10% FCS, 100 U/ml penicillin, and 100 mg/ml streptomycin (Invitrogen). The confluent cells were used at *passages 4–6*. We confirmed that >99% of cells were positive for α-smooth muscle actin and showed the typical "hill-and-valley" morphology.

Cell proliferation assays. [^{3}H]thymidine incorporation was used to measure cell proliferation in DA SMCs. The SMCs were reseeded into a 24-well culture plate at an initial density of 1×10^5 cells per well for 24 h before serum starvation with DMEM containing 0.5% FCS. Cells were then incubated with or without nitrendipine (1 μM), kurtoxin (1 μM), and efonidipine (3 μM) for 16 h in the starvation medium before addition of 1 μCi of [*methyl*-^{3}H]thymidine (specific activity 5 Ci/mM; Amersham International, Bucks, UK) for 4 h at 37°C. After fixation with 1.0 ml of 10% trichloroacetic acid, the cells were solubilized with 0.5 ml of 0.5 M NaOH and then neutralized with 0.25 ml of 1 N HCl. A liquid scintillation counter was used to measure [^{3}H]thymidine incorporation. Data obtained from triplicate wells were averaged.

Generation of expression construct for spliced variant of rat α_{1C}-subunit. The 220-bp fragment containing a 75-bp insertion of the spliced variant of rat VDCC α_{1C}-subunit was extracted from the 453-bp PCR fragment using *Xho* I and *Sph* I restriction enzymes. Then the 220-bp fragment was introduced into the *Xho* I/*Sph* I site of the pcDNA3.1(+)-based expression construct of the rat brain 1C subunit (rbCII; kindly supplied by Dr. T. P. Snutch) (35). The sequence of the expression construct was confirmed by direct sequencing analysis.

Electrophysiological recordings. $Ca_V1.2$ (rbCII; GenBank accession no. M67515) or its mutant was transiently expressed in BHK6 cells, which stably express β_1- and $\alpha_{2\delta}$-subunits. Transfection was carried out with a transfection reagent (FuGene 6, Roche), as previously described (43).

Electrophysiological recordings were performed in the whole cell patch-clamp configuration using a patch/whole cell-clamp amplifier (Axopatch 200B, Axon Instruments) and an analog-to-digital converter (Digidata 1200, Axon Instruments) (43). Data acquisition was performed with pCLAMP7 software (Axon Instruments). Signals were filtered at 5 kHz. Capacitative currents were electrically compensated. The P/4 protocol (pCLAMP7) was used for leak subtraction. Ca^{2+} currents and Ba^{2+} currents (I_{Ba}) through $Ca_V1.2$ (rbCII) Ca^{2+} channels expressed in BHK6 cells were measured as previously described (27). The external solution contained (in mM) 137 NaCl, 5.4 KCl, 1 $MgCl_2$, 10 HEPES, and 10 glucose, with 2 $CaCl_2$ or $BaCl_2$ as a charge carrier; pH was adjusted to 7.4 with NaOH at room temperature. The resistance of the patch electrode was 2–2.5 MΩ when it was filled with the pipette solution containing (in mM) 120 $CsMeSO_4$, 20 TEA-Cl, 14 EGTA, 5 Mg-ATP, 5 Na_2 creatine phosphate, 0.2 GTP, and 10 HEPES, with pH adjusted to 7.3 with CsOH at room temperature. All experiments were carried out at room temperature.

The half-activation potential ($V_{h\text{-}act}$) was estimated by fitting the current-voltage (*I-V*) relations (curves) to the following equation by an interactive nonlinear regression fitting procedure

$$I = (V_m - V_{rev}) * G_{max} * \{1/[1 + \exp(V_m - V_{h\text{-}act})/k]\}$$

where V_m is membrane potential, V_{rev} is reversal potential, k is slope factor, and G_{max} is maximum conductance.

Half-inactivation voltage ($V_{h\text{-}inact}$) was estimated by fitting the steady-state inactivation curves to the following equation

$$I = I_{min} + (I_{max} - I_{min})/[1 + \exp(V_{h\text{-}inact} - V)/k]$$

where I_{max} and I_{min} are maximum and minimum plateau currents, respectively, and k is slope factor.

Statistical analysis. Values are means ± SE. Student's unpaired *t*-tests and unpaired ANOVA followed by the Student-Newman-Keuls test were used for statistical analysis. $P < 0.05$ was considered statistically significant.

RESULTS

Multiple transcripts of VDCC α_1-, $\alpha_{2\delta}$-, and β-subunits in rat DA. Semiquantitative RT-PCR analyses revealed that, among voltage-dependent L-type Ca^{2+} channel subunits, α_{1C}- and α_{1D}-subunit mRNAs were expressed in the DA and the aorta, whereas neither α_{1F}- nor α_{1S}-subunit transcript was detected (Fig. 1*A*). The α_{1C}-subunit transcripts were amplified as two bands, 378 bp (the expected size) and 453 bp, in the RT-PCR products. The 378-bp band was confirmed as the reported VDCC α_{1C}-subunit, and the 453-bp band was identified as a novel spliced variant of the rat VDCC α_{1C}-subunit by sequencing analysis. Another spliced variant of α_{1C}-subunit in the human, which displayed oxygen-sensitive opening of the channel, was recently identified (11). However, we could not detect this spliced variant in DA, aorta, and genomic DNA in the rat by RT-PCR using $Ca_V1.2$ (α_{1C})-2 primers, although we could detect its expression in human right ventricle (data not shown). The expression of VDCC α_{1A} (P/Q-type)-, α_{1B} (N-type)-, and α_{1E} (R-type)-subunits was not detected in the DA by semiquantitative RT-PCR (data not shown).

The transcripts of all T-type Ca^{2+} channel α_1-subunits, α_{1G}, α_{1H}, and α_{1I}, were detected in the DA and aorta (Fig. 1*B*). In our PCR conditions, expression of the α_{1G}-isoform was highest and expression of the α_{1H}-isoform was lowest in the DA among T-type Ca^{2+} channel α_1-subunits. Expression of α_{1I} was decreased from e21 in the DA and from *day 0* in the aorta.

The transcripts of all four $\alpha_{2\delta}$-subunits were detected in the DA and aorta (Fig. 1*C*). Transcripts of all four β-subunits were detected in the DA and aorta (Fig. 1*D*). Among them, β_3-subunit mRNA was highly expressed by semiquantitative RT-PCR during development in the DA and aorta. Expression of β_3-subunit mRNA was not changed during development. Expression of β_1-subunit mRNA was not detected in adult aorta.

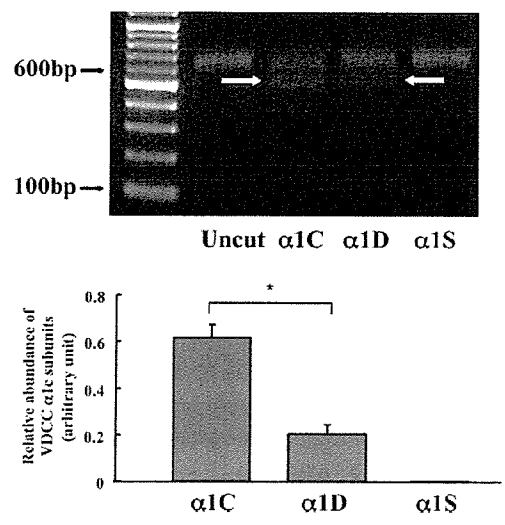

Fig. 2. Relative abundance of L-type Ca^{2+} channel α_1-subunits in DA at e21. Uncut lane shows a single band corresponding to fragments obtained after RT-PCR; α_{1C}, α_{1D}, and α_{1S} lanes show fragments obtained after restriction digest with enzymes. Digested fragments are indicated by arrows. Digested fragment was detected more in α_{1C}- than in α_{1D}-subunit. No digested fragment was detected in α_{1S}-subunit. Values for α_{1C}- and α_{1D}-subunits were obtained from the value into which elements digested by each enzyme were divided by amount of uncut PCR product using densitometry. The α_{1C}-subunit is the most abundant of the L-type Ca^{2+} channel subunits. *$P < 0.01$.

Expression β_2- and β_4-subunit mRNA was higher in the fetus than that in neonates on *day 0*.

VDCC α_{1C}-subunit was a predominant transcript of L-type Ca^{2+} channel subunits in rat DA. Using restriction enzyme analysis as previously reported (29), we determined relative abundance of HVA Ca^{2+} channel mRNA. The digested fragments were detected only in the α_{1C}- and α_{1D}-subunit lanes (Fig. 2), which is consistent with the result from semiquantitative RT-PCR. The values of α_{1C}- and α_{1D}-subunits were obtained when the value into which elements digested by each enzyme was divided by the amount of uncut PCR product. The density of the digested fragment was significantly higher in the α_{1C}- than in the α_{1D}-subunit lane, indicating that the α_{1C}-subunit is the most abundant transcript among L-type Ca^{2+} channel subunits.

Protein expression of α_{1C}-, α_{1D}-, α_{1G}-, and β_3-subunits in the DA. Protein expression of α_{1C}-, α_{1D}-, α_{1G}-, and β_3-subunits was examined by immunoblotting analysis (Fig. 3). Although the expression level of α_{1C}-subunit mRNA was higher in the DA than in the fetal aorta, the expression level of α_{1C}-subunit protein in the DA was comparable with that in the aorta at e21 and much less than that in the adult atrium and aorta. Protein expression of the α_{1D}-subunit was similarly detected in the DA and aorta at e21, but not in the adult aorta. The level of α_{1G}-subunit protein expression was high in the DA and aorta at e21 and undetectable in the adult aorta. We also detected β_3-subunit protein expression in the DA at e21.

In addition, we examined the localization of α_{1C}-, α_{1D}-, and α_{1G}-subunit proteins in the DA at e21 by immunostaining with anti-α_{1C}, -α_{1D}, and -α_{1G} (Fig. 3*B*). Strong immunoreaction of α_{1C}- and α_{1G}-subunits and moderate immunoreaction of the α_{1D}-subunit were found in SMCs in the DA. Especially, the α_{1G}-subunit was strongly expressed in the region of intimal thickening of the DA, which is clearly distinguished by Elastica stain.

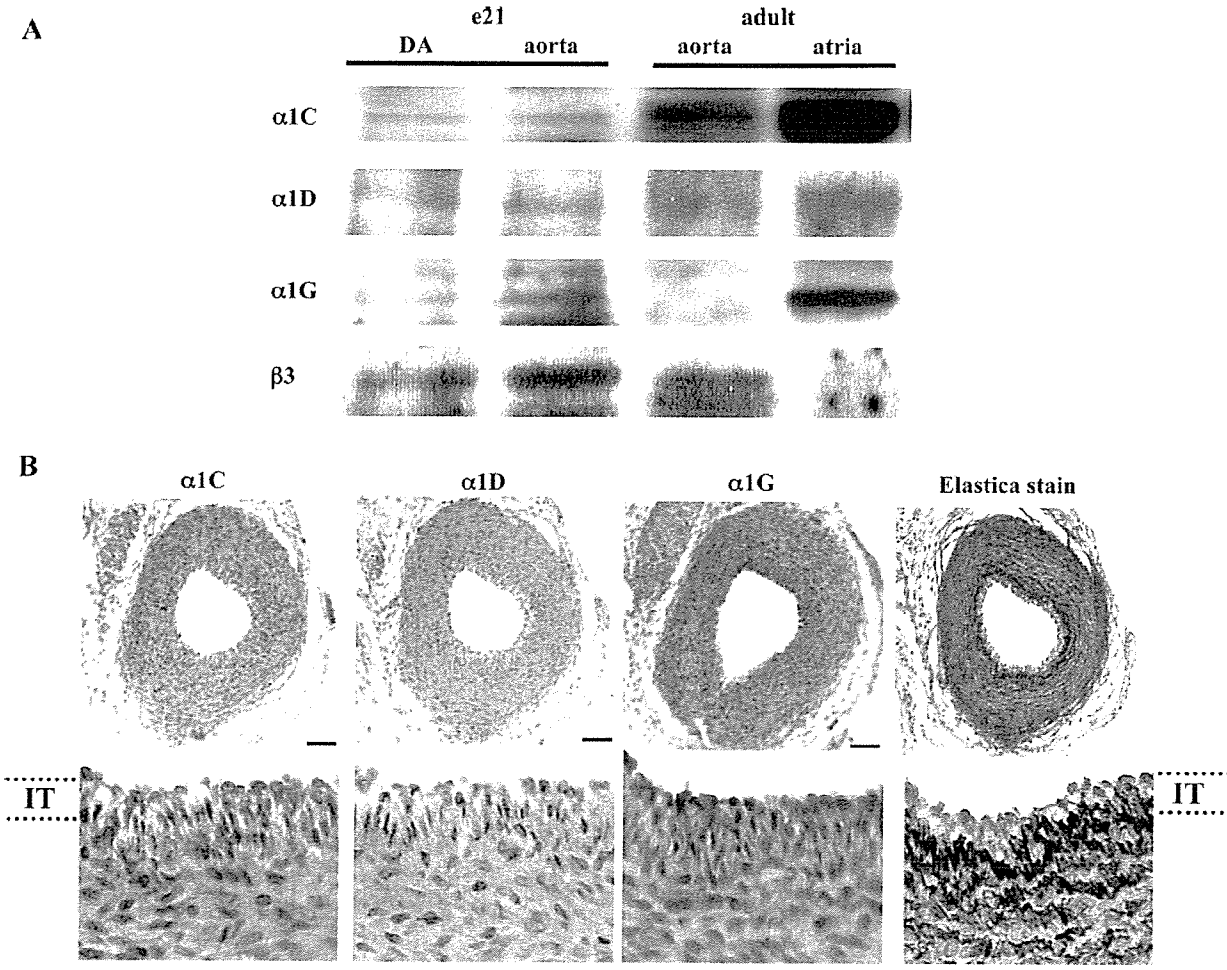

Fig. 3. *A*: expression of α_{1C}-, α_{1D}-, α_{1G}-, and β_3-subunit protein in rat DA, aorta, and atrium by immunoblotting. Membrane proteins from rat tissues were separated by SDS-PAGE, together with prestained molecular weight markers, and subjected to immunoblot analysis with each subunit-selective antibody. Expression level of α_{1C}-subunit protein was comparable in DA and aorta at e21 and much less in DA than in adult atrium. Expression of α_{1D}-subunit was similarly detected in DA and aorta at e21. Expression of α_{1G}-subunit protein was high in DA and aorta at e21 and undetectable in adult aorta. Expression of β_3-subunit was high in DA at e21. *B*: DA at e21 immunostained with anti-α_{1C}, -α_{1D}, and -α_{1G}. Elastica stain identified the boundary of intimal cushion formation. High-magnification (×4) image of the region of intimal cushion formation is shown at *bottom*. Strong immunoreaction of α_{1C}-subunit and mild immunoreaction of α_{1D}-subunit were ubiquitously found in DA. Strong α_{1G}-subunit immunoreaction was especially found at the region of intimal thickening (IT) in DA. Scale bar, 100 μm.

Effects of development and maternally administered vitamin A on expression of VDCC α_1-subunit transcripts. Although the expression levels of α_{1C}-subunit mRNA were not changed in the DA during development, a significant decrease in the expression level of α_{1C}-subunit mRNA in the aorta resulted in a higher expression of α_{1C}-subunit mRNA in the DA than in the aorta after e21 (Fig. 4*A*). Maternally administered vitamin A significantly increased the expression levels of α_{1C}-subunit mRNA at *day 0* ($P < 0.01$; Fig. 4*B*).

Expression of α_{1G}-subunit mRNA was 25–120 times higher in perinatal vessels than in the adult aorta (Fig. 4*C*). The expression was upregulated in the DA during development. The level of α_{1G}-subunit mRNA was significantly higher in the DA than in the aorta at *day 0*. Maternally administered vitamin A significantly upregulated the expression of α_{1G}-subunit mRNA at all developmental stages ($P < 0.001$; Fig. 4*D*).

Effects of L- and T-type VDCCs on SMC proliferation in DA. We used a specific L-type VDCC blocker (nitrendipine), a specific T-type VDCC blocker (kurtoxin), and an L- and T-type VDCC blocker (efonidipine) to investigate a role for VDCCs in SMC proliferation in the DA. Significant inhibition of [^{3}H]thymidine incorporation was observed in rat DA SMCs treated with 1 μM nitrendipine, 3 μM efonidipine, or 1 μM kurtoxin compared with untreated SMCs (Fig. 5). The inhibition was the strongest in SMCs treated with 3 μM efonidipine, suggesting that the additive inhibitory effect of efonidipine on cell proliferation is due to the blockade of L- and T-type VDCCs in rat DA SMCs.

A novel spliced variant of the α_{1C}-subunit was highly expressed in adult lung and fetal arteries. As demonstrated above, using RT-PCR with $Ca_v1.2$ (α_{1C})-1 primers, we found a novel alternatively spliced isoform of the α_{1C}-subunit in the DA and aorta (Table 1). The PCR products were subcloned into a pCRII vector (Invitrogen) and sequenced. We reported the nucleotide sequence in the EMBL/GenBank nucleotide sequence databases (accession no. AY323810; Fig. 6*A*). The spliced variant contained a 26-amino acid insertion into the I-II cytoplasmic linker that interacts with the β-subunit of α_{1C} (Fig. 6*B*). During the course of the present study, homologs of this variant have been reported in other species. Figure 6*C* shows

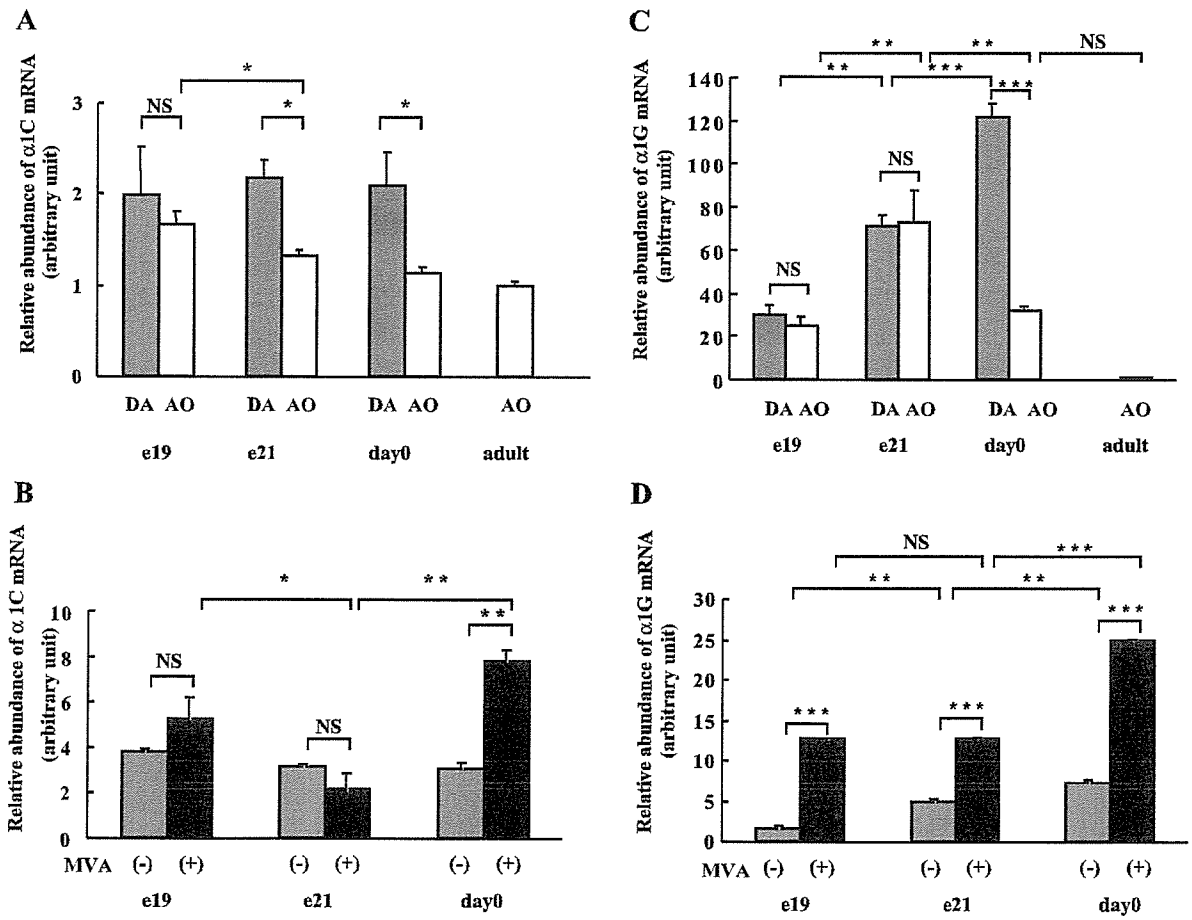

Fig. 4. *A*: developmental changes in expression of α_{1C}-subunit mRNA. Expression level of α_{1C}-subunit mRNA was higher in DA than in aorta (AO) at e21 and *day 0*. Expression level was not changed in DA during development but was decreased in aorta from e19 to e21. $^*P < 0.05$. NS, not significant. *B*: effects of maternally administered vitamin A (MVA) on expression of α_{1C}-subunit mRNA in DA. Levels of α_{1C}-subunit mRNA were not changed in DA during development and were significantly increased with vitamin A only at *day 0*. $^*P < 0.05$; $^{**}P < 0.01$. *C*: developmental changes in expression of α_{1G}-subunit mRNA. Transcripts for α_{1G}-subunit were increased during development in DA. Abundance of α_{1G}-subunit mRNA was significantly greater in DA than in aorta at *day 0*. $^{**}P < 0.01$; $^{***}P < 0.001$. *D*: effects of maternally administered vitamin A on expression of α_{1G}-subunit mRNA in DA. Expression of α_{1G}-subunit mRNA was upregulated during development and significantly higher than with vitamin A at any developmental stage. $^{**}P < 0.01$; $^{***}P < 0.001$.

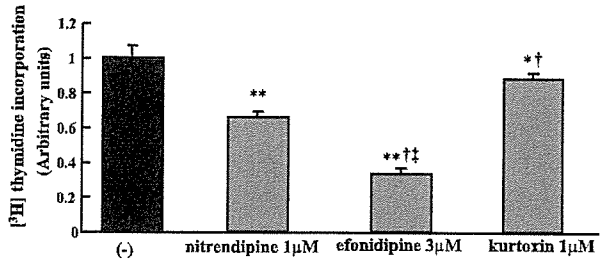

Fig. 5. Effects of VDCC blockers on [^{3}H]thymidine uptake of DA smooth muscle cells. [^{3}H]thymidine incorporation in groups treated with nitrendipine, efonidipine, and kurtoxin was decreased compared with that in control group in 0.1% FCS-containing medium. Treatment of DA smooth muscle cells with efonidipine resulted in additional reduction of [^{3}H]thymidine uptake compared with nitrendipine or kurtoxin treatment. Experiments were performed 3 times independently in duplicate. Significantly different from control: $^*P < 0.01$, $^{**}P < 0.0001$. †Significantly different from nitrendipine ($P < 0.01$). ‡Significantly different from kurtoxin ($P < 0.01$).

that amino acid sequence homology between the rat and other species (mouse, rabbit, and human) is very high (100%, 92%, and 88%, respectively).

We characterized the novel spliced isoform of rat α_{1C}-subunit. Figure 7*A* shows the expression the spliced variant of α_{1C}-subunit mRNA and protein by semiquantitative RT-PCR and immunoblotting analyses. The PCR product migrating 453 bp was the spliced variant of the α_{1C}-subunit and the 378-bp band indicated the reported α_{1C}-subunit. A relatively high intensity of the 453-bp band was detected in the DA and the aorta. Using the specific antibody against the spliced variant of the α_{1C}-subunit, we also found a high level of expression of the variant protein in arteries, including the DA, and less expression in the adult heart.

By quantitative RT-PCR analyses, the spliced variant transcript was expressed most abundantly in the adult lung (data not shown), less in the fetal arteries, and least in the adult arteries. In other adult tissues, the expression level of α_{1C}-subunit mRNA, including this spliced variant, was very low (data not shown). The ratio of the abundance of the spliced variant to the conventional α_{1C}-isoform was measured by quantitative RT-PCR (see MATERIALS AND METHODS). The proportion of the spliced variant and nonspliced α_{1C}-isoform was almost invariable (1–1.5) among the lung, DA, and aorta. Furthermore, we examined the developmental changes in the expression of the spliced variant of the α_{1C}-subunit transcript in the DA and aorta (Fig. 7*B*). The level of the spliced variant α_{1C}-subunit mRNA peaked at e21 in the DA. After birth, the level of the spliced variant α_{1C}-subunit mRNA was higher in the DA than in the aorta.

Localization of the spliced variant of the α_{1C}-subunit in the DA at e21 was examined by immunostaining with anti-α_{1C}-subunit splicing variant (Fig. 7*C*). Strong immunoreaction was found in the region of intimal thickening of the DA (Fig. 7*C*, *right*), whereas immunoreaction of the conventional α_{1C}-isoform was ubiquitously expressed in the whole layers of the DA (Fig. 3*B*).

Fig. 6. *A*: alignment of nucleotide sequence of rat Ca^{2+} channel α_{1C}-subunit (GenBank accession no. AF394938) and novel spliced variant (GenBank accession no. AY323810). Spliced variant consists of a 75-bp insertion. *B*: amino acid sequence of rat Ca^{2+} channel α_{1C}-subunit. Spliced variant contains a 25-amino acid insertion into the I-II cytoplasmic linker that interacts with the β-subunit of α_{1C}. *C*: comparison of amino acid sequence of novel α_{1C}-subunit alternatively spliced isoform among several species. Sets of conservative or unconservative residues are indicated in bold or light font, respectively. Amino acid sequence is highly conserved among species.

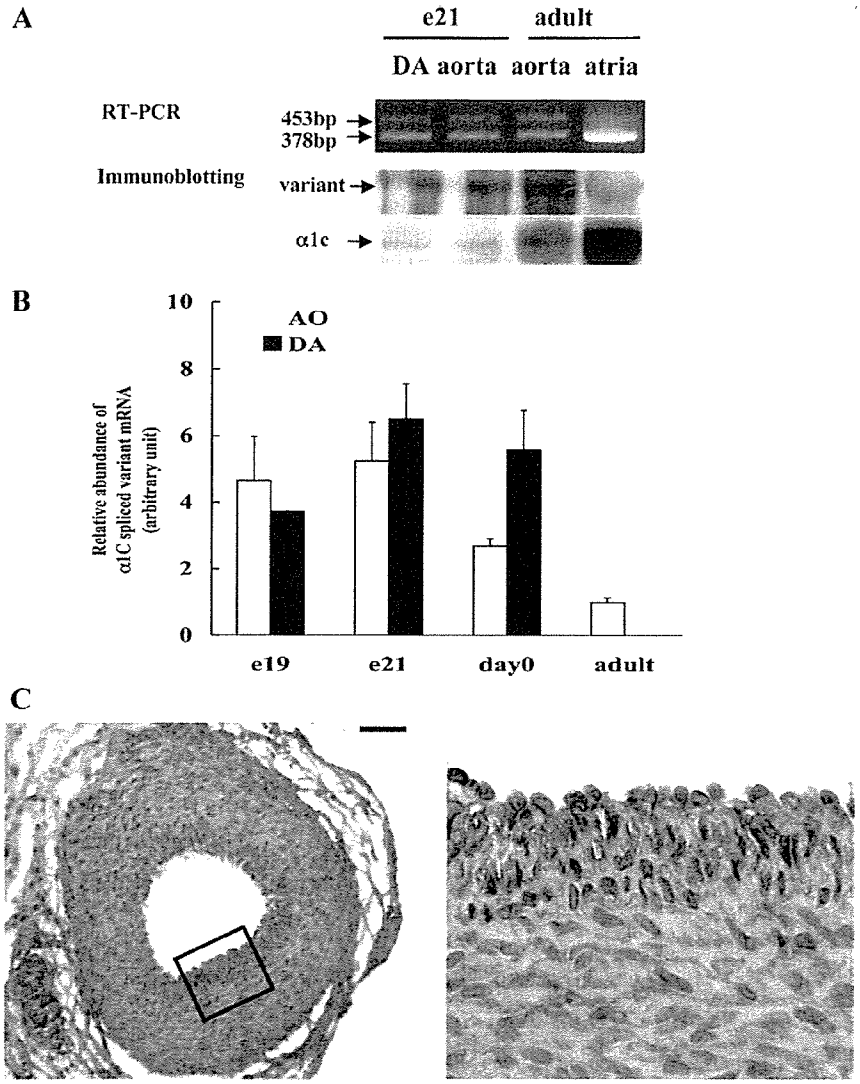

Fig. 7. *A*: expression of splicing variant of α_{1C}-subunit confirmed by semiquantitative RT-PCR and immunoblotting analyses. Band migrating at 453 bp is spliced variant of α_{1C}-subunit; smaller band is nonspliced α_{1C}-isoform. Immunoblotting analysis revealed that spliced variant of α_{1C}-subunit was highly expressed in vascular smooth muscle, including DA, at mRNA and protein levels. *B*: relative abundance of spliced variant of α_{1C}-subunit mRNA measured by quantitative RT-PCR. Level of spliced variant of α_{1C}-subunit mRNA is highly expressed in DA and aorta in the fetus. *C*: immunoreaction of splicing variant of α_{1C}-subunit was found in smooth muscle cells of DA at e21. Strong immunoreaction was found in region of intimal thickening. Scale bar, 100 μm. High-magnification (×4) image of region enclosed in rectangle at *left* is shown at *right*.

We examined whether the DA variant exerts any differences in the gating kinetics of the Ca^{2+} channel. Activation and inactivation kinetics of I_{Ba} were not significantly different between rbCII and the DA variant (Fig. 8*A*). The expression level at the surface membrane, estimated as the density of I_{Ba}, did not differ between the two groups, even though the individual cell showed a wide variety of I_{Ba} density, as is often the case with a transient expression experiment (Fig. 8*B*). The *I-V* relations of rbCII and the DA variant were almost superimposable (Fig. 8*C*). $V_{h\text{-}act}$ of rbCII and the DA variant were -15.4 ± 1.9 mV ($n = 9$) and -14.5 ± 1.2 mV ($n = 7$), respectively (not statistically significant). The steady-state inactivation curves could be slightly shifted toward the depolarized direction in the DA variant, but $V_{h\text{-}inact}$ was not significantly different: -33.3 ± 1.0 mV ($n = 9$) and -31.5 ± 1.7 mV ($n = 6$), respectively.

DISCUSSION

Ca^{2+} influx through VDCCs plays an important role in vascular myogenic reactivity and tone (4, 8, 26). To our knowledge, the present study demonstrated the first complete characterization of the expression of VDCC subtype mRNAs in the DA. Tristani-Firouzi et al. (38) demonstrated that activation of L-type, but not T-type, VDCCs plays a major role in oxygen-sensitive contraction in the DA. Takizawa et al. (37) demonstrated that an L-type VDCC blocker, verapamil, inhibits its spontaneous closure of the DA in newborn rats. Therefore, the abundant expression of α_{1C}-subunit mRNA in the DA suggested that the α_{1C}-subunit is mainly responsible for the influx of Ca^{2+} that induces contraction of the DA after birth.

We also found that all T-type VDCCs were expressed in the DA. The most dominant isoform among T-type VDCCs in the DA is the α_{1G}-subunit, with an expression level 25–120 times higher in fetal vessels than in adult aorta, which is consistent with previous reports showing that T-type VDCCs are predominantly expressed in the early stages of differentiation of many embryonic and neonatal tissues (2, 9, 12, 21). The expression of α_{1G}-subunit mRNA was significantly upregulated by maternal administration of vitamin A. In the DA, α_{1G}-subunit protein was highly localized in the region of intimal thicken-

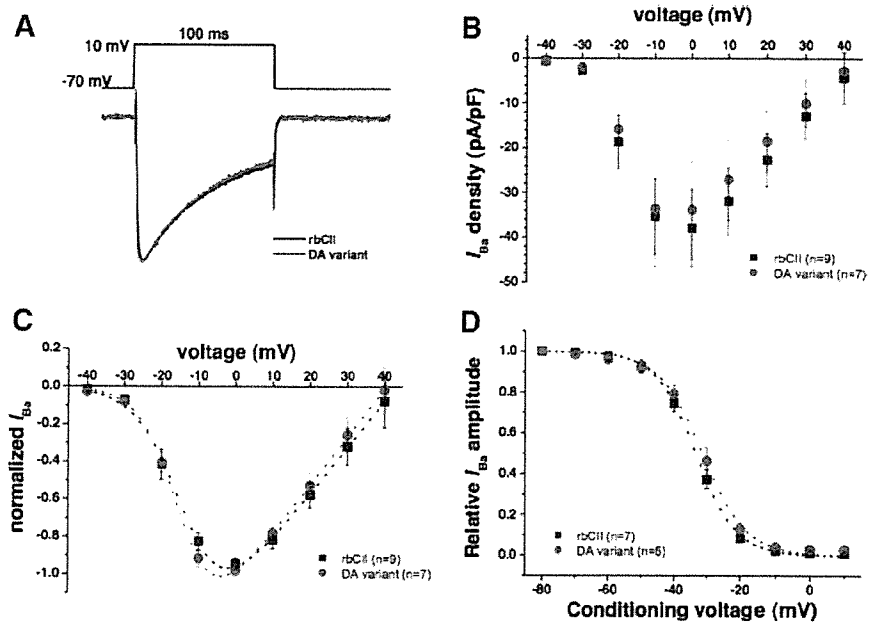

Fig. 8. *A*: Ba^{2+} current (I_{Ba}) traces of rat brain 1C subunit (rbCII) and the DA variant. Peak normalized currents were averaged and superimposed. Pulse protocol is indicated above current traces. *B*: voltage dependence of I_{Ba} density of DA variant and rbCII. *C*: current-voltage (*I-V*) relations (curve) of rbCII and the DA variant. Amplitude of I_{Ba} was normalized to peak value in each recording and averaged. *D*: steady-state inactivation curves of rbCII and the DA variant. Test pulse to 0 mV for 100 ms was applied after conditioning pulse for 5 s to the respective voltages ranging from −80 to 10 mV in 10-mV steps and for 25 ms at −70 mV. Values are means ± SE.

ing. Although the abundant expression of the α_{1G}-subunit suggests that the α_{1G}-subunit plays an important role in the DA, the physiological role of T-type VDCCs in smooth muscle contraction has been obscure. However, Ca^{2+} influx through the α_{1H}-subunit has been recently identified to be essential for normal relaxation of coronary arteries (4). Therefore, T-type VDCCs may play a similar role in the DA, rather than in oxygen-sensitive contraction (38). Further investigation is necessary to test the possibility.

In addition to the regulation of vascular tone, L- and T-type VDCCs are also known to regulate differentiation (14, 17), proliferation (19, 36, 44), migration (7, 31), and gene expression (41) in vascular SMCs. In the present study, we found that L- and T-type Ca^{2+} channel blockers significantly inhibited [^{3}H]thymidine incorporation in DA SMCs, suggesting that L- and T-type VDCCs promote cell proliferation in the DA. Moreover, we found that BAY K 8644, an L-type VDCC activator, increased DA SMC migration in a dose-dependent manner (unpublished data). A previous study demonstrated that the blockade of T-type, but not L-type, VDCCs prevented neointima formation after vascular injury (32), which shares a molecular mechanism of intimal thickening similar to that of the DA. Our present results, however, indicate that L- and T-type VDCCs are involved in intimal thickening in the DA in different ways.

Previous studies demonstrated that responses of the DA to oxygen and indomethacin, a prostaglandin H synthase inhibitor, are blunted at e19 and are apparent at e21 (24, 25). In this study, the expression level of α_{1C}-subunit mRNA at e19 was similar to that at e21 or *day 0*. Therefore, the expression level of the α_{1C}-subunit was not considered the cause of the blunted response of the DA to oxygen and indomethacin at e19. One may argue that an oxygen-sensitive signal is activated at near term (e21) to increase the activity of VDCCs. In this sense, vitamin A and/or retinoic acid signaling is a candidate for the activator of oxygen sensitivity, because the retinoic acid response element is strongly expressed in the mouse DA (6), and maternally administered vitamin A accelerated development of the oxygen-sensing mechanism of the rat DA (42). Previous studies have also demonstrated that retinoic acid upregulated α_{1C}-subunit L-type Ca^{2+} channel expression in vascular SMCs (13) and H_9C_2 cardiac myoblast cell lines (22). Although vitamin A upregulated the expression of α_{1C}-subunit mRNA in the DA only at *day 0*, it would be of great interest that vitamin A and/or retinoic acid signal may enhance the activity of VDCCs in the DA.

We found a novel spliced variant of the α_{1C}-subunit in the rat. The spliced variant contained a 25-amino acid insertion into the I-II cytoplasmic linker. The interaction between the cytoplasmic I-II linker of α_{1C}- and β-subunits is known to modulate channel opening (16). During the preparation of this manuscript, Liao et al. (18) reported the same spliced variant of the α_{1C}-subunit. They demonstrated that the spliced variant of the α_{1C}-subunit exhibited a hyperpolarized shift in voltage-dependent activation and the *I-V* relation in HEK 293 cells. However, we did not find a difference in basic electrophysiological channel properties between the conventional and the spliced variant of α_{1C}-subunits. Although we do not explain an exact reason for the conflicting results between two studies, the discrepancy may be due to the different conditions of the experiments: we used rat cDNA and the β_1-subunit, whereas Liao et al. used human cDNA and the β_2-subunit. Although we did not find a difference in basic channel properties between the conventional and the spliced variant of α_{1C}-subunits, we found the distinct expression pattern of the spliced variant in the DA. The spliced variant was strongly expressed in neointimal thickening of the DA, where SMCs exhibit more proliferating and migrating characters (33, 34). In addition, we found that expression of the spliced variant mRNA was significantly increased in the lung of monocrotaline-treated rats (unpublished data). These results suggest a distinct role for the spliced variant in adaptation to various physiological and/or pathological signals.

In conclusion, multiple VDCC subunits were identified in the DA, and, in particular, α_{1C}- and α_{1G}-subunits were predominant in the DA. The expression of α_{1C}- and α_{1G}-subunit mRNAs was higher in the DA than in the aorta and was significantly upregulated by maternal administration of vitamin A. We found a novel spliced variant of the α_{1C}-subunit gene that may play a specific role in Ca^{2+} entry in the lung and fetal arteries. Our study could be an important first step in identification of the molecular basis of Ca^{2+} channel function in the DA. On the basis of our results, further study would identify the physiological relevance between mRNA levels and Ca^{2+} channel function in the DA.

ACKNOWLEDGMENTS

We are grateful to Takayo Musuda, Mayumi Watanabe, and Chikako Usami for excellent technical assistance and animal care. Efonidipine was kindly provided by Nissan Chemical Industries (Saitama, Japan).

GRANTS

This work was partly supported by the Mother and Child Health Foundation (S. Minamisawa), 2005 Strategic Research Project Grant K17014 of Yokohama City University (S. Minamisawa), the Yokohama Foundation for Advancement of Medical Science (U. Yokoyama and T. Akaike), and a Grant-in-Aid for Scientific Research from the Japanese Society for the Promotion of Science (S. Adachi-Akahane).

REFERENCES

1. **Arikkath J and Campbell KP.** Auxiliary subunits: essential components of the voltage-gated calcium channel complex. *Curr Opin Neurobiol* 13: 298–307, 2003.
2. **Bijlenga P, Liu JH, Espinos E, Haenggeli CA, Fischer-Lougheed J, Bader CR, and Bernheim L.** T-type α_{1H} Ca^{2+} channels are involved in Ca^{2+} signaling during terminal differentiation (fusion) of human myoblasts. *Proc Natl Acad Sci USA* 97: 7627–7632, 2000.
3. **Catterall WA.** Structure and regulation of voltage-gated Ca^{2+} channels. *Annu Rev Cell Dev Biol* 16: 521–555, 2000.
4. **Chen CC, Lamping KG, Nuno DW, Barresi R, Prouty SJ, Lavoie JL, Cribbs LL, England SK, Sigmund CD, Weiss RM, Williamson RA, Hill JA, and Campbell KP.** Abnormal coronary function in mice deficient in α_{1H} T-type Ca^{2+} channels. *Science* 302: 1416–1418, 2003.
5. **Coceani F and Olley PM.** The control of cardiovascular shunts in the fetal and perinatal period. *Can J Physiol Pharmacol* 66: 1129–1134, 1988.
6. **Colbert MC, Kirby ML, and Robbins J.** Endogenous retinoic acid signaling colocalizes with advanced expression of the adult smooth muscle myosin heavy chain isoform during development of the ductus arteriosus. *Circ Res* 78: 790–798, 1996.
7. **Corsini A, Bonfatti M, Quarato P, Accomazzo MR, Raiteri M, Sartani A, Testa R, Nicosia S, Paoletti R, and Fumagalli R.** Effect of the new calcium antagonist lercanidipine and its enantiomers on the migration and proliferation of arterial myocytes. *J Cardiovasc Pharmacol* 28: 687–694, 1996.
8. **Davis MJ and Hill MA.** Signaling mechanisms underlying the vascular myogenic response. *Physiol Rev* 79: 387–423, 1999.
9. **Del Toro R, Levitsky KL, Lopez-Barneo J, and Chiara MD.** Induction of T-type calcium channel gene expression by chronic hypoxia. *J Biol Chem* 278: 22316–22324, 2003.
10. **De Reeder EG, Poelmann RE, van Munsteren JC, Patterson DF, and Gittenberger-de Groot AC.** Ultrastructural and immunohistochemical changes of the extracellular matrix during intimal cushion formation in the ductus arteriosus of the dog. *Atherosclerosis* 79: 29–40, 1989.
11. **Fearon IM, Varadi G, Koch S, Isaacsohn I, Ball SG, and Peers C.** Splice variants reveal the region involved in oxygen sensing by recombinant human L-type Ca^{2+} channels. *Circ Res* 87: 537–539, 2000.
12. **Ferron L, Capuano V, Deroubaix E, Coulombe A, and Renaud JF.** Functional and molecular characterization of a T-type Ca^{2+} channel during fetal and postnatal rat heart development. *J Mol Cell Cardiol* 34: 533–546, 2002.
13. **Gollasch M, Haase H, Ried C, Lindschau C, Morano I, Luft FC, and Haller H.** L-type calcium channel expression depends on the differentiated state of vascular smooth muscle cells. *FASEB J* 12: 593–601, 1998.
14. **Gollasch M, Lohn M, Furstenau M, Nelson MT, Luft FC, and Haller H.** Ca^{2+} channels, "quantized" Ca^{2+} release, and differentiation of myocytes in the cardiovascular system. *J Hypertens* 18: 989–998, 2000.
15. **Hofmann F, Lacinova L, and Klugbauer N.** Voltage-dependent calcium channels: from structure to function. *Rev Physiol Biochem Pharmacol* 139: 33–87, 1999.
16. **Hohaus A, Poteser M, Romanin C, Klugbauer N, Hofmann F, Morano I, Haase H, and Groschner K.** Modulation of the smooth-muscle L-type Ca^{2+} channel α_1 subunit ($\alpha_{1C\text{-}b}$) by the β_{2a} subunit: a peptide which inhibits binding of β to the I-II linker of α_1 induces functional uncoupling. *Biochem J* 348: 657–665, 2000.
17. **Kuga T, Kobayashi S, Hirakawa Y, Kanaide H, and Takeshita A.** Cell cycle-dependent expression of L- and T-type Ca^{2+} currents in rat aortic smooth muscle cells in primary culture. *Circ Res* 79: 14–19, 1996.
18. **Liao P, Yu D, Lu S, Tang Z, Liang MC, Zeng S, Lin W, and Soong TW.** Smooth muscle-selective alternatively spliced exon generates functional variation in $Ca_V1.2$ calcium channels. *J Biol Chem* 279: 50329–50335, 2004.
19. **Lijnen P, Fagard R, and Petrov V.** Mibefradil-induced inhibition of proliferation of human peripheral blood mononuclear cells. *J Cardiovasc Pharmacol* 33: 595–604, 1999.
20. **McCleskey EW.** Calcium channels: cellular roles and molecular mechanisms. *Curr Opin Neurobiol* 4: 304–312, 1994.
21. **McCobb DP, Best PM, and Beam KG.** Development alters the expression of calcium currents in chick limb motoneurons. *Neuron* 2: 1633–1643, 1989.
22. **Menard C, Pupier S, Mornet D, Kitzmann M, Nargeot J, and Lory P.** Modulation of L-type calcium channel expression during retinoic acid-induced differentiation of H9C2 cardiac cells. *J Biol Chem* 274: 29063–29070, 1999.
23. **Minamisawa S, Oshikawa J, Takeshima H, Hoshijima M, Wang Y, Chien KR, Ishikawa Y, and Matsuoka R.** Junctophilin type 2 is associated with caveolin-3 and is down-regulated in the hypertrophic and dilated cardiomyopathies. *Biochem Biophys Res Commun* 325: 852–856, 2004.
24. **Momma K, Nakanishi T, and Imamura S.** Inhibition of in vivo constriction of fetal ductus arteriosus by endothelin receptor blockade in rats. *Pediatr Res* 53: 479–485, 2003.
25. **Momma K, Toyono M, and Miyagawa-Tomita S.** Accelerated maturation of fetal ductus arteriosus by maternally administered vitamin A in rats. *Pediatr Res* 43: 629–632, 1998.
26. **Moosmang S, Schulla V, Welling A, Feil R, Feil S, Wegener JW, Hofmann F, and Klugbauer N.** Dominant role of smooth muscle L-type calcium channel $Ca_V1.2$ for blood pressure regulation. *EMBO J* 22: 6027–6034, 2003.
27. **Naguro I, Nagao T, and Adachi-Akahane S.** Ser^{1901} of α_{1C} subunit is required for the PKA-mediated enhancement of L-type Ca^{2+} channel currents but not for the negative shift of activation. *FEBS Lett* 489: 87–91, 2001.
28. **Nakanishi T, Gu H, Hagiwara N, and Momma K.** Mechanisms of oxygen-induced contraction of ductus arteriosus isolated from the fetal rabbit. *Circ Res* 72: 1218–1228, 1993.
29. **Plant TD, Schirra C, Katz E, Uchitel OD, and Konnerth A.** Single-cell RT-PCR and functional characterization of Ca^{2+} channels in motoneurons of the rat facial nucleus. *J Neurosci* 18: 9573–9584, 1998.
30. **Rabinovitch M.** Cell-extracellular matrix interactions in the ductus arteriosus and perinatal pulmonary circulation. *Semin Perinatol* 20: 531–541, 1996.
31. **Ruiz-Torres A, Lozano R, Melon J, and Carraro R.** L-calcium channel blockade induced by diltiazem inhibits proliferation, migration and F-actin membrane rearrangements in human vascular smooth muscle cells stimulated with insulin and IGF-1. *Int J Clin Pharmacol Ther* 41: 386–391, 2003.
32. **Schmitt R, Clozel JP, Iberg N, and Buhler FR.** Mibefradil prevents neointima formation after vascular injury in rats. Possible role of the blockade of the T-type voltage-operated calcium channel. *Arterioscler Thromb Vasc Biol* 15: 1161–1165, 1995.
33. **Slomp J, Gittenberger-de Groot AC, Glukhova MA, Conny van Munsteren J, Kockx MM, Schwartz SM, and Koteliansky VE.** Differentiation, dedifferentiation, and apoptosis of smooth muscle cells during the development of the human ductus arteriosus. *Arterioscler Thromb Vasc Biol* 17: 1003–1009, 1997.
34. **Slomp J, Gittenberger-de Groot AC, Koteliansky VE, Glukhova MA, Bogers AJ, and Poelmann RE.** Cytokeratin expression in human arteries

pertinent to intimal thickening formation in the ductus arteriosus. *Differentiation* 61: 305–311, 1997.

35. **Snutch TP, Tomlinson WJ, Leonard JP, and Gilbert MM.** Distinct calcium channels are generated by alternative splicing and are differentially expressed in the mammalian CNS. *Neuron* 7: 45–57, 1991.
36. **Sperti G and Colucci WS.** Calcium influx modulates DNA synthesis and proliferation in A7r5 vascular smooth muscle cells. *Eur J Pharmacol* 206: 279–284, 1991.
37. **Takizawa T, Oda T, Arishima K, Yamamoto M, Masaoka T, Somiya H, Akahori F, and Shiota K.** A calcium channel blocker verapamil inhibits the spontaneous closure of the ductus arteriosus in newborn rats. *J Toxicol Sci* 19: 171–174, 1994.
38. **Tristani-Firouzi M, Reeve HL, Tolarova S, Weir EK, and Archer SL.** Oxygen-induced constriction of rabbit ductus arteriosus occurs via inhibition of a 4-aminopyridine-, voltage-sensitive potassium channel. *J Clin Invest* 98: 1959–1965, 1996.
39. **Tsien RW, Lipscombe D, Madison DV, Bley KR, and Fox AP.** Multiple types of neuronal calcium channels and their selective modulation. *Trends Neurosci* 11: 431–438, 1988.
40. **Uemura N, Ohkusa T, Hamano K, Nakagome M, Hori H, Shimizu M, Matsuzaki M, Mochizuki S, Minamisawa S, and Ishikawa Y.** Down-regulation of sarcolipin mRNA expression in chronic atrial fibrillation. *Eur J Clin Invest* 34: 723–730, 2004.
41. **Wamhoff BR, Bowles DK, McDonald OG, Sinha S, Somlyo AP, Somlyo AV, and Owens GK.** L-type voltage-gated Ca^{2+} channels modulate expression of smooth muscle differentiation marker genes via a Rho kinase/myocardin/SRF-dependent mechanism. *Circ Res* 95: 406–414, 2004.
42. **Wu GR, Jing S, Momma K, and Nakanishi T.** The effect of vitamin A on contraction of the ductus arteriosus in fetal rat. *Pediatr Res* 49: 747–754, 2001.
43. **Yamaguchi S, Okamura Y, Nagao T, and Adachi-Akahane S.** Serine residue in the IIIS5-S6 linker of the L-type Ca^{2+} channel α_{1C} subunit is the critical determinant of the action of dihydropyridine Ca^{2+} channel agonists. *J Biol Chem* 275: 41504–41511, 2000.
44. **Yang Z, Noll G, and Luscher TF.** Calcium antagonists differently inhibit proliferation of human coronary smooth muscle cells in response to pulsatile stretch and platelet-derived growth factor. *Circulation* 88: 832–836, 1993.